ELSEVIER

Chemical Engineering Science 62 (2007) 246–255

Chemical Engineering Science

www.elsevier.com/locate/ces

Numerical study of segregation using a new drag force correlation for polydisperse systems derived from lattice-Boltzmann simulations

R. Beetstra, M.A. van der Hoef*, J.A.M. Kuipers

Department of Science and Technology, University of Twente, P.O. Box 217, 7500 AE Enschede, The Netherlands

Available online 3 September 2006

Abstract

Discrete particle simulations of a segregating system are performed using various drag relations and boundary conditions, and compared to experiments. The boundary conditions on the walls are found to have a large influence on the segregation behaviour of the fluidised bed, where no-slip conditions result in unrealistic flow patterns. A polydispersity factor, which was recently derived on the basis of lattice-Boltzmann (LBM) simulations, is found to have a major effect on the segregation velocity and the final degree of segregation. The best agreement with experimental results is obtained with drag relations that were recently proposed based on LBM-simulations in combination with the aforementioned polydispersity factor.

Keywords: Fluidisation; Segregation; Discrete particle model; Drag force; Boundary conditions

1. Introduction

Fluidised bed reactors combine a thorough contact between solid particles and a fluid with excellent heat and mass transfer properties, and are therefore often encountered in the chemical, petrochemical, metallurgical and food processing industries. In the fluidised state, the drag force from the fluid on the particles is so large that it outbalances gravity and the particles 'float' in the reactor. This enhances mixing in the reactor, and generally results in a lower pressure drop over the reactor.

When the particles in a fluidised bed differ in size and/or density, segregation may occur. This phenomenon is caused by a difference in drag force and/or gravity, with the result that one type of particles fluidises more easily than the other. The particles that are easily fluidised (small or light particles) will move to the top section of the bed (flotsam), while the other particles settle in the bottom region (jetsam). In gas fluidised beds segregation usually occurs only at fluidisation velocities not far from the minimum fluidisation velocity of the larger or heavier particles. At higher gas velocities bubbles cause a more thorough mixing in the bed, thereby disturbing segregation patterns. Liquid fluidisation is usually more homogeneous than gas fluidisation, which is the reason why segregation can occur at higher velocities as well in this type of process.

In practical applications segregation can be very important, since particles in a reactor are almost never monodisperse. In polymerisation or granulation processes high diameter ratios may occur, which strongly influences the hydrodynamic behaviour and mixing in the reactor. On the other hand, it is essential to control the size distribution of the end product and to prevent clogging of the reactor. Therefore, a model that is able to predict segregation accurately will be a very useful tool in industrial applications.

Hoomans (1999), Goldschmidt et al. (2003) and Bokkers et al. (2004) have shown that it is very difficult to predict segregation processes in fluidised suspensions accurately with the current CFD-models, in particular when the rate of this segregation is used as a criterion and not merely the final state. This suggests that the drag models require some modification for use in binary or polydisperse systems.

Van der Hoef et al. (2005) and Beetstra et al. (2006) showed, using lattice-Boltzmann (LBM) simulations, that the drag force on particles in a mixture is indeed different from the drag force on the same particle in a monodisperse system with the same

* Corresponding author. Tel.: +31 53 489 2953; fax +31 53 489 2882.
E-mail address: m.a.vanderhoef@tnw.utwente.nl (M.A. van der Hoef).

0009-2509/$ - see front matter © 2006 Elsevier Ltd. All rights reserved.
doi:10.1016/j.ces.2006.08.054

porosity and Reynolds number. On the basis of these simulations, a correction factor for the monodisperse drag force was suggested, which takes into account the bidispersity of the system. In this paper the results of discrete particle simulations of a segregating system using this correction factor will be compared to similar simulations without the correction term. The influence of the expression for the average drag force is also tested, as well as the influence of boundary conditions.

2. Discrete particle model (DPM)

The discrete particle model that is used in this work was originally developed by Hoomans et al. (1996). Below an overview of the main equations is given, while a more extensive description can be found in Hoomans (1999) and Van der Hoef et al. (2006).

In the discrete particle model, the gas phase is described by the volume-averaged Navier–Stokes equations. The continuity equation for the gas phase is given by

$$\frac{\partial(\varepsilon\rho_g)}{\partial t} + \nabla\cdot\varepsilon\rho_g\mathbf{u} = 0, \tag{1}$$

where ε is the porosity of the system, ρ_g the density of the gas and $\mathbf{u}$ the gas velocity. The momentum equation for the gas phase is given by:

$$\frac{\partial(\varepsilon\rho_g\mathbf{u})}{\partial t} + \nabla\cdot\varepsilon\rho_g\mathbf{u}\mathbf{u} = -\varepsilon\nabla P - \mathbf{S} - \nabla\cdot\varepsilon\tau_g + \varepsilon\rho_g\mathbf{g}. \tag{2}$$

In this equation P is the pressure, τ_g the viscous stress tensor and $\mathbf{g}$ the acceleration due to gravity. $\mathbf{S}$ is a source term that describes the momentum exchange of the gas with the solid phase. Note that two-way coupling is important for a realistic description at high solids volume fractions such as studied in this work.

The particle dynamics are based on Newton's equations of motion, which for particle p reads

$$m_p\frac{\mathrm{d}\mathbf{v}_p}{\mathrm{d}t} = m_p\mathbf{g} + \frac{V_p\beta}{(1-\varepsilon)}(\mathbf{u}-\mathbf{v}_p) - V_p\nabla P, \tag{3}$$

where m_p, V_p and $\mathbf{v}_p$ are the mass, volume and velocity of the particle, respectively. The second term on the right hand side is the drag force, where β is the inter-phase momentum exchange coefficient, which is directly related to the (dimensionless) drag force (see Section 2.1). The source term in Eq. (2) depends on the same friction coefficient, and can formally be written as

$$\mathbf{S} = \frac{1}{V}\int\sum_{p=1}^{N}\frac{V_p\beta}{(1-\varepsilon)}(\mathbf{u}-\mathbf{v}_p)\delta(\mathbf{r}-\mathbf{r}_p)\,\mathrm{d}V, \tag{4}$$

which represents the change in momentum per unit volume for a typical control volume V.

Particle collisions are handled through the soft-sphere model. This is a linear spring/dash-pot model where the force on a colliding particle is determined by the amount of (fictitious) overlap it has with other particles. Multiple collisions are possible in this model. Contrary to a hard-sphere model that is event-driven (the system evolves from collision to collision), the soft-sphere model uses a fixed time step. Therefore, the soft-sphere model is preferred in cases where many collisions occur, e.g. in very dense systems.

2.1. Drag force in DPM

The size of the computational cells in the discrete particle model typically exceeds the diameter of the particles, and therefore a closure model for the drag force has to be implemented. This is done via the inter-phase momentum exchange coefficient β, which is defined as

$$\mathbf{F}_d = \frac{V_p\beta}{(1-\varepsilon)}(\mathbf{u}-\mathbf{v}_p). \tag{5}$$

The local porosity and gas velocity necessary for the evaluation of this equation are obtained through a volume-weighted averaging procedure Hoomans (1999). The force of a particle on the gas phase is distributed to the surrounding cells by the same technique.

In this paper the drag force is denoted as the normalised drag force F (normalised by the Stokes–Einstein drag $3\pi\mu\,\mathrm{d}U$), which is related to β by

$$F = \frac{F_d}{3\pi\mu\,\mathrm{d}U} = \frac{d^2\beta}{18\mu\varepsilon(1-\varepsilon)}. \tag{6}$$

In this equation μ is the fluid viscosity and U is the superficial velocity through the system.

Most numerical models use the empirical equation by Ergun (1952) for porosities up to 0.8, combined with the drag correlation by Wen and Yu (1966) for higher porosities (see also Enwald et al., 1996). Bokkers et al. (2004) compared results obtained with this equation to simulations using the drag relation that was derived from LBM simulations by Hill et al. (2001). The latter equation was shown to give results that were in better agreement with experiments as compared to simulations where the empirical models were used. Beetstra et al. (2006) derived another drag relation from LBM results, which is slightly more accurate than the relation of Hill et al. (2001) and valid over a wider range of Reynolds numbers. This relation was derived from simulations where the porosity was varied from 0.4 to 0.9, and the Reynolds number from $Re = 0.1$ to 1000. In total, 35 different combinations of porosity and Reynolds number were used in monodisperse systems. Apart from this, bidisperse systems were studied, where the porosity was varied from 0.35 to 0.9; the Reynolds number from Re=0.1 to 500; the diameter ratio from 0.25 to 0.7 and several mixture compositions were studied, leading to a total of 150 different systems. The particles were given a velocity (the same for all particles in the system), and after steady state had been reached the drag force on each particle was measured. For each of the systems, a number of simulations with different configurations and velocities was studied (up to thirty simulations per system for the monodisperse systems and five for the mixtures), to eliminate the effect of the configuration on the drag force.

Table 1
Relations used in the discrete particle simulations to determine the average (or monodisperse) drag force

Ergun/Wen and Yu	$F = \frac{150}{18}\frac{(1-\varepsilon)}{\varepsilon^2} + 1.75\frac{Re}{18\varepsilon^2}$	$\varepsilon < 0.8$
	$F = \frac{Re}{24} C_d(Re)\varepsilon^{-3.65}$	$\varepsilon > 0.8$
	$C_D(Re) = \frac{24}{Re}(1 + 0.15Re^{0.687})$	$Re < 1000$
	$C_D(Re) = 0.44$	$Re > 1000$
Hill et al.	$F = F_0 + \frac{1}{2}F_3 Re$	
	$F_0 = 10\frac{\phi}{(1-\phi)^2}$	$\varepsilon < 0.6$
	$F_0 = (1-\phi)\frac{1 + (3/\sqrt{2})\sqrt{\phi} + (135/64)\phi\ln\phi + 16.14\phi}{1 + 0.681\phi - 8.48\phi^2 + 8.16\phi^3}$	$\varepsilon > 0.6$
	$F_3 = 0.0673 + 0.212\phi + \frac{0.0232}{(1-\phi)^5}$	
Beetstra et al.	$F = 10\frac{1-\varepsilon}{\varepsilon^2} + \varepsilon^2(1 + 1.5\sqrt{1-\varepsilon}) + \frac{0.413Re}{24\varepsilon^2}\left(\frac{\varepsilon^{-1} + 3\varepsilon(1-\varepsilon) + 8.4Re^{-0.343}}{1 + 10^{3\phi}Re^{-0.5-2\phi}}\right)$	
	where $\phi = 1-\varepsilon$, $Re = \frac{\rho_g U\langle d\rangle}{\mu}$	

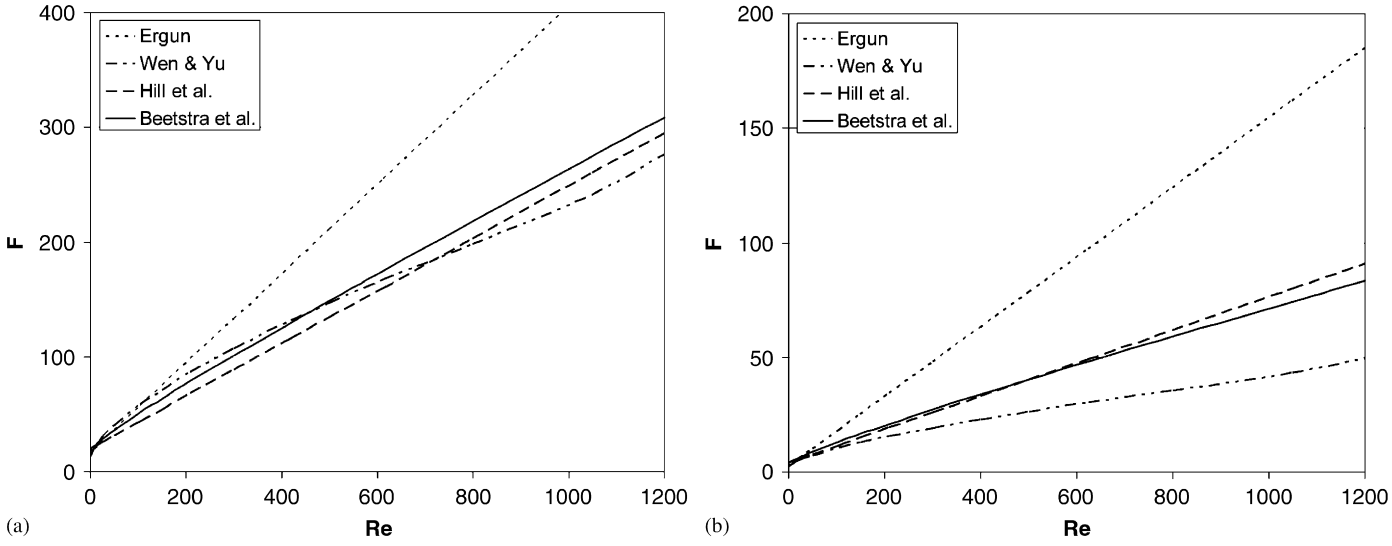

Fig. 1. Predictions for the normalised drag force as a function of Reynolds number calculated with the various equations used in this work: (a) ε=0.5; (b) ε=0.8.

It was found that the average drag force for mixtures can be described by the same equation as for monodisperse systems, when the average diameter $\langle d\rangle$ is used. This average diameter is defined by $\langle d\rangle = (\sum \chi_i/d_i)^{-1}$, where χ_i the mass fraction of particles of type i (i.e., $\chi_i = N_i d_i^3/(\sum_i N_i d_i^3)$, with N_i the number of particles of type i). The results of the LBM simulations for monodisperse systems agreed very well with literature results using similar methods (Hill et al., 2001). On the basis of our data we have proposed a new drag force relation which is on average within 3% of the simulation data. For an overview of the monodisperse drag relations we refer to Table 1. The predictions for the normalised drag force calculated with the various drag correlations are compared in Fig. 1 for two different porosities. The drag relations of Hill et al. (2001) and Beetstra et al. (2006) (which were both derived from LBM simulation results) predict very similar values, while the empirical Ergun equation always predicts a higher drag force. For dense systems the Wen and Yu equation corresponds reasonably well with the equations derived from LBM simulations, however, for dilute systems the deviations become larger, where the Wen and Yu equation predicts much lower values for the drag force. From 1(b) it is also clear that the transition from Ergun to Wen and Yu at $\varepsilon = 0.8$ is by no means a smooth one, since the two relations can differ by as much as a factor of 3 at that porosity.

If for a binary or polydisperse mixture the individual drag force on a particle of type i is given by $\mathbf{F}_{d,i}$, then we define the normalised drag force F_i as

$$F_i = F_{d,i}/3\pi\mu d_i U,$$

where d_i is the diameter of type i particles. Van der Hoef et al. (2005) and Beetstra et al. (2006) showed that F_i can be substantially different from the normalised drag force F on the same particle in a monodisperse system with equal porosity and Reynolds number. A simple argument for this effect is that in a binary configuration, the local porosity of the smaller particles is somewhat higher than the average porosity (larger pores surrounding the particle, where by pore we mean the open space in between the particles), whereas for the larger particles it is lower. The small particles thus experience a smaller drag force, while the force on the larger particles is larger than what would be expected on the basis of the average porosity. Based on theoretical considerations, a relation was presented to correct for the effect of polydispersity, which depends on the porosity, diameter ratio and composition of the mixture:

$$F_i = F(\varepsilon, \langle Re\rangle)(\varepsilon y_i + (1-\varepsilon)y_i^2), \tag{7}$$

where

$$y_i = \frac{d_i}{\langle d\rangle}, \quad \langle Re\rangle = \frac{\rho_g U \langle d\rangle}{\mu}, \quad \frac{1}{\langle d\rangle} = \sum_i \frac{\chi_i}{d_i},$$

with χ_i is the mass fraction of species i. In Eq. (7), $F(\varepsilon, \langle Re\rangle)$ is the normalised drag force of a monodisperse system at the same porosity and at Reynolds number $\langle Re\rangle$. Eq. (7) was found to match LBM simulation results within 5% for y_i in the range $0.7 < y_i < 1.4$; however, outside this range—thus for more extreme diameter ratio's—the deviation becomes larger than 10%. This can be remedied by including a third order term

$$F_i = (\varepsilon y_i + (1-\varepsilon)y_i^2 + 0.064\varepsilon y_i^3)F, \tag{8}$$

which provides the best fit to all simulation data, up to diameter ratio's of 1:4. In this paper we will study the effect of both the drag relation F and the correction term on segregation phenomena in numerical models of bidisperse fluidised beds.

2.2. Boundary conditions

Apart from the effect of the drag relation, the influence of boundary conditions imposed in the simulations is studied as well. Near a solid wall, the friction with that wall will usually be so large that the fluid acquires the same velocity as the wall. This so-called no-slip boundary condition, implies that for gas–fluidised beds the gas velocity at the bed walls will be zero. Another possibility is that the fluid experiences no friction from a boundary and is thus allowed to move freely along this boundary, which is called free-slip boundary condition, for the velocity gradient at the interface will be zero at equilibrium. A typical example of such a boundary condition is found at the gas–liquid interface. In an experimental fluidised bed the gas flow near the walls shows no-slip behaviour. However, this does not mean that this is the obvious choice for the boundary conditions to be imposed in a DPM-simulation. This is illustrated by Fig. 2, which shows the typical velocity profile near the wall in a porous system (solid line) as a function of the distance from the wall. At the wall, no-slip conditions apply and the velocity is equal to zero. In the bulk of the bed, the velocity is equal to the minimum fluidisation velocity U_{mf} (when the effect of bubbles are neglected). In the boundary layer, which typically has a thickness of the order of one particle diameter, the fluid velocity increases rapidly. However, since the porosity near the walls is higher than in the bulk of the bed (less resistance to flow), the velocity may increase to even higher values than U_{mf} in this region, resulting in the overshoot shown in the figure. Also shown are the free-slip approximation and no-slip approximation. It is important to realise that the z-velocity is calculated half a cell length away from the wall. In reality the velocity at that position will be equal to the bulk velocity, since a computational cell in the discrete particle model usually measures at least 4–10 particle diameters. The velocity closer to the wall is calculated from linear interpolation between this point and the wall velocity, which is zero in the case of no-slip conditions and equal to the velocity in the first cell when free-slip conditions are used. Therefore, in case of no-slip conditions the profile may not be steep enough, resulting in velocities that are too low compared to what is found in reality, and particles in this region will experience a lower drag force. In case of free-slip conditions the fluid velocity at the wall is obviously not correct. However, since there are no particles located directly at the wall, this does not necessarily influence the particle behaviour very much. The best choice of boundary conditions in each simulation will depend on vari-

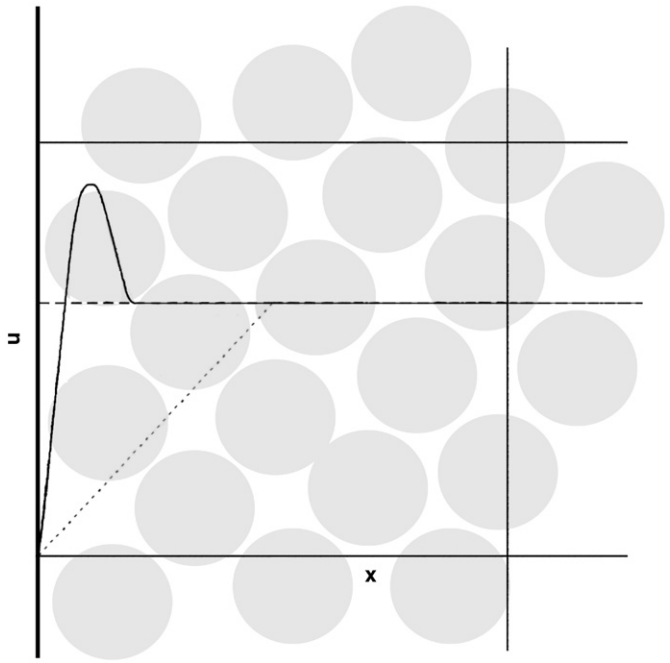

Fig. 2. Qualitative representation of the gas velocity profile in a computational cell next to the wall in a dense bed. The solid line is the realistic situation; the dotted and dashed lines represent the no-slip and free-slip approximations in the discrete particle model, respectively.

ables like the cell size in relation to particle diameter and the porosity.

3. Simulation setup

The segregation simulations presented here are based on the experiments performed by Goldschmidt et al. (2003), where glass particles with diameters of 1.5 and 2.5 mm were fluidised with air in a pseudo-2D column. The mixture consists of 25% small particles and 75% large particles, and the fluidisation velocity is 1.30 m/s. The various parameters in the simulations are chosen such to agree with the experimental system as close as possible, and are given in Table 2.

The degree of segregation in the experiment was determined with an optical method Goldschmidt et al. (2003): pictures that were taken during the experiment were divided in cells, and the intensities of red (large particles) and yellow (small particles) were determined for each cell. From the fraction of large and small particles in the cell the degree of segregation s could then be determined, which is defined as

$$s = \frac{S - 1}{S_{\max} - 1}, \tag{9}$$

where $S = \langle h_{\text{small}} \rangle / \langle h_{\text{large}} \rangle$ and $S_{\max} = (x_{\text{large}} + 1)/x_{\text{large}}$, $\langle h_i \rangle$ being the average height of particles of type i and x_{large} the volume fraction of large particles. Thus, for a completely mixed system $s = 0$, and for a completely segregated system $s = 1$. In the simulations the same quantitative measure for segregation is determined via the z-coordinates of all particles.

The experiments were repeated three times, which differed slightly in the degree of segregation. Values for the degree of segregation that are shown in the figures in this section are the average of these three experiments. The simulation were performed using different drag models and boundary conditions. An overview of the various combinations is shown in Table 3. Note that we also performed simulations with the Ergun and Hill, Koch and Ladd-drag models with the new correction for polydispersity, since this correction factor can in principle be coupled to any monodisperse drag relation.

Table 2
Settings in the segregation simulations

Width	0.15 m	
Depth	0.015 m	
Height	0.45 m	
Gas velocity	1.3 m/s	
	Coarse grid	Fine grid
Cells in x-direction	15	30
Cells in y-direction	1	1
Cells in z-direction	45	90
Particles	Large	Small
Number	17940	27720
Diameter	2.5 mm	1.5 mm
Density	2525 kg/m^3	2525 kg/m^3
Coefficient of normal restitution	0.97	0.97
Coefficient of friction	0.10	0.10
Coefficient of tangential restitution	0.33	0.33

Table 3
Drag models and boundary conditions in the segregation simulations

Run	Drag model	Correction	Grid	Boundary
1	Beetstra et al. (BHK)	Yes	Coarse	Free-slip
2	Beetstra et al. (BHK)	Yes	Coarse	No-slip
3	Beetstra et al. (BHK)	Yes	Fine	No-slip
4	Beetstra et al. (BHK)	No	Coarse	Free-slip
5	Beetstra et al. (BHK)	No	Coarse	No-slip
6	Beetstra et al. (BHK)	No	Fine	No-slip
7	Ergun/Wen and Yu (Ergun)	No	Coarse	Free-slip
8	Ergun/Wen and Yu (Ergun)	Yes	Coarse	Free-slip
9	Hill et al. (HKL)	No	Coarse	Free-slip
10	Hill et al. (HKL)	Yes	Coarse	Free-slip

4. Results

4.1. Visual observations

Figs. 3–6 show snapshots of the experiment and simulations. Fig. 3 shows typical bubble patterns that occur in each simulation, the others illustrate the evolution of the segregation in time. A qualitative comparison shows that the bubble patterns in the experiment and the simulations are very different, where the bubbles in the simulations are much smaller. In the no-slip simulations all bubbles move towards the side walls of the bed, whereas in the experiment and free-slip simulations they also pass through the centre. The size of the bubbles has a strong influence on the particle dynamics, most notably in the top layer. In the simulations the top layer stays more or less at its place, whereas in the experiments it is moving vigorously with every new eruption of a bubble. A more quantitative comparison reveals that the bubble frequency (measured from bed expansion characteristics) is higher in the simulations, ranging from 2.5 to 3.1 Hz, while this was 1.9 Hz in the experiments of Goldschmidt et al. (2003). In simulation number 4 an even higher frequency of 3.7 Hz was observed for some period of time, which was mainly due to some vigorous motions in the segregated top layer.

In the simulations with no-slip boundary conditions and a coarse grid, many small particles are located in the vicinity of the side walls of the bed. Animations of the simulation reveal that a flow pattern of (small) particles is moving up through the center of the bed in the wake of bubbles, followed by a downwards motion from the segregated layer along the sides of the bed, a phenomenon which does not appear as such in the experiments. This is related to the bubble pattern that was discussed previously: in the experiment large bubbles disturb circulation patterns that are formed, so that the particles have no chance to move downwards near the walls. A closer look into this phenomenon will be taken in the next section.

4.2. Effect of grid and boundary conditions

The degree of segregation as a function of time in simulations using different boundary conditions and grid sizes is shown in Fig. 7, and compared to the experimental value (average

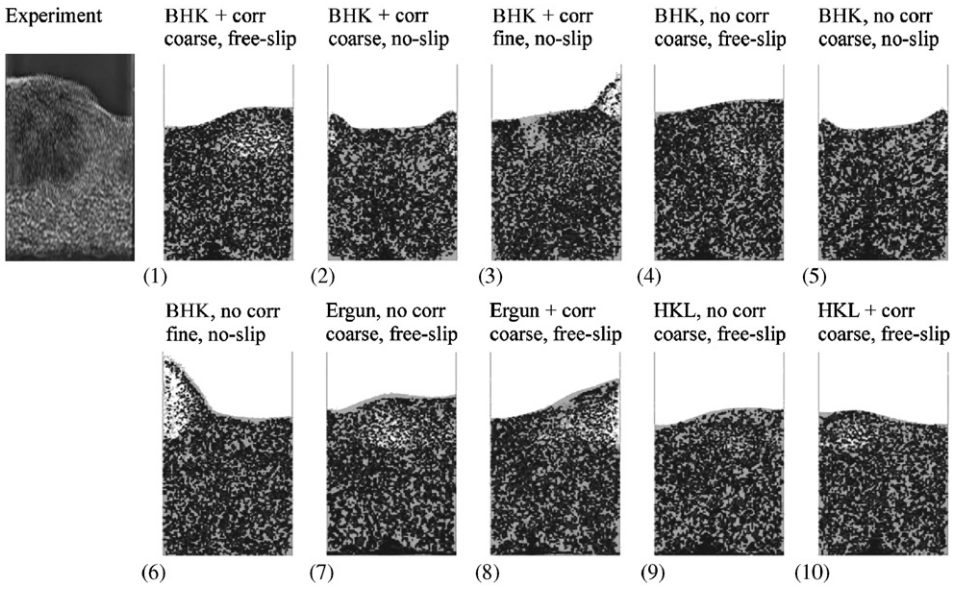

Fig. 3. Snapshots from segregation experiment and simulations showing typical bubble patterns. All snapshots are taken shortly after start-up ($t = 2$–6 s). Numbers refer to Table 3.

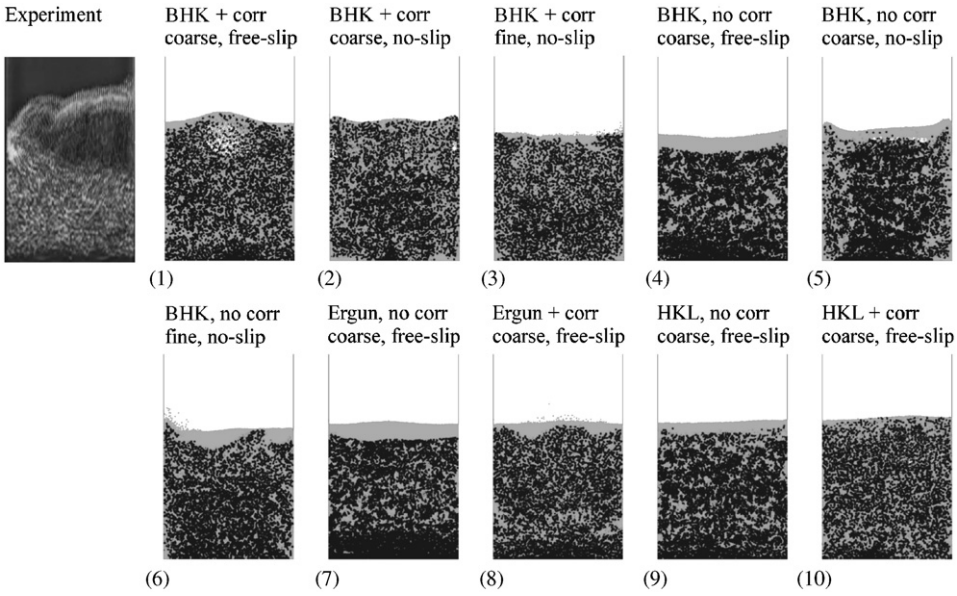

Fig. 4. Snapshots from segregation experiment and simulations showing degree of segregation at $t = 10$ s. Numbers refer to Table 3.

of three experiments). The segregation rate is much higher in simulations with free-slip conditions than in simulations with no-slip conditions. The reason is that in the no-slip simulations the fluid velocity near the walls is smaller, so that the drag in the cells near the wall is also lower than in the rest of the bed. As a result, the drag force acting on particles close to these walls will not balance gravity anymore, so particles that have reached the top layer move down again along the sides with a lower segregation rate as a result.

Fig. 8 shows the degree of segregation in the lateral direction (x-dimension) s_{lat}, which is defined in the same way as the degree of axial segregation s, where instead of the average height of the particles of type i the average x-position relative to the centre of the bed is taken. The difference between the simulations is obvious: in the simulations with no-slip boundary conditions the lateral segregation is much larger than in the experiments and the free-slip simulations. This effect is even more pronounced in simulations using the Ergun and Hill drag models and no-slip boundaries that are not shown here. The simulations with no-slip conditions performed on a finer grid are found to yield better results than the coarse grid simulations, which can be explained by the fact that the zone near the wall with a reduced gas velocity is smaller. In general it can be concluded that the grid size has a larger influence on the simulation results than the boundary conditions. This is underscored by the snapshots in Figs. 3–6: in the fine grid

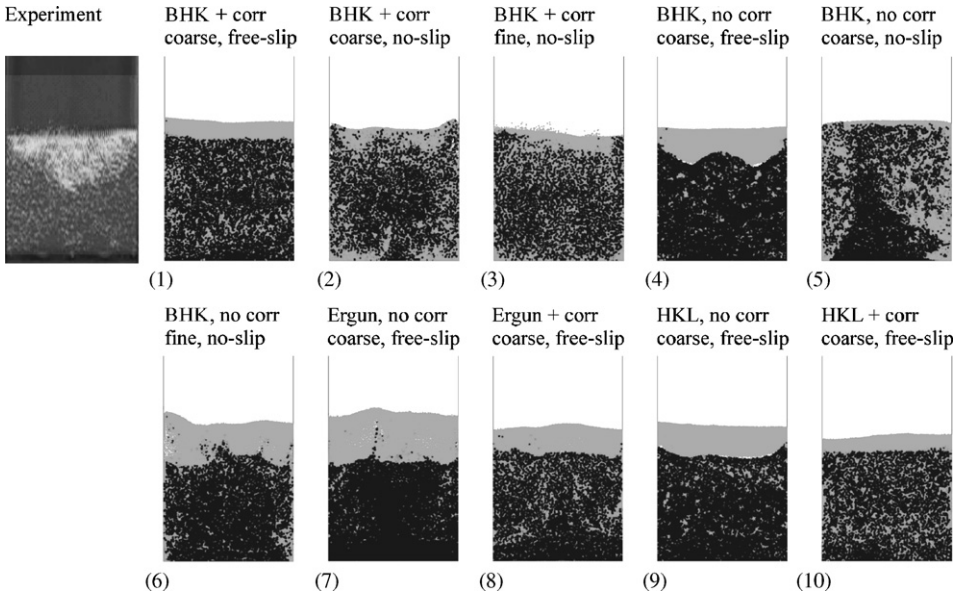

Fig. 5. Same as Fig. 4, but now at $t = 30$ s.

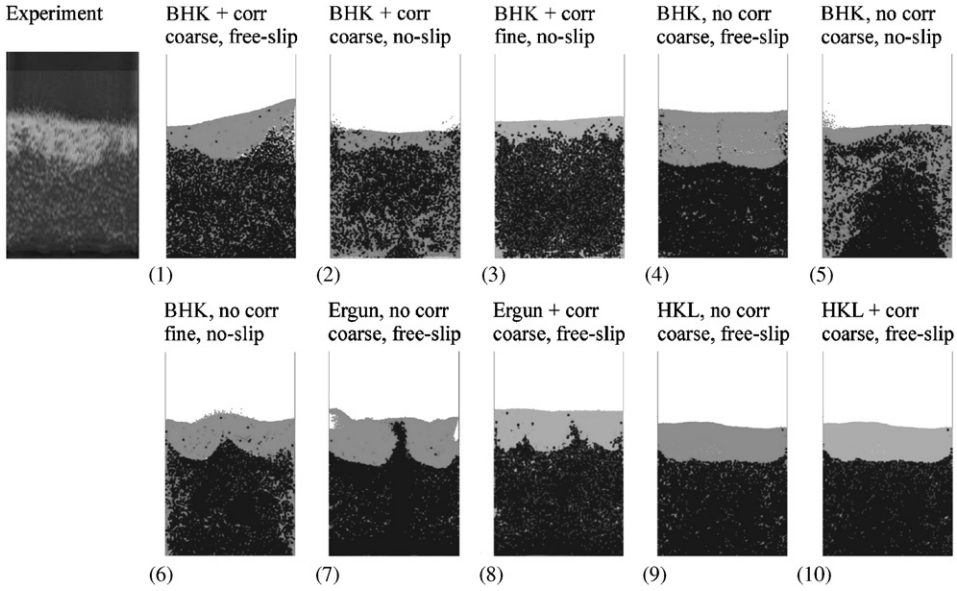

Fig. 6. Same as Fig. 4, but now at $t = 50$ s.

simulations there is still an effect of the system wall on the particle distribution, which is not found in the experiment, whereas this effect is not visible in the free slip simulation. Animations of the simulations and experiment make this even more clear, in this case a circulation pattern of (small) particles moving upwards through the centre of the bed and downwards along the walls was observed, which was not visible in the experiments.

4.3. Effect of the polydispersity factor and drag factor

When the correction factor for polydispersity, Eq. (7) or (8), is taken into account, the drag on the small particles in the system becomes smaller while the larger particles experience a larger drag than in a simulation without this correction factor. Thus, the smaller particles move to the top zone at a slower rate, while the larger particles have a lower downward velocity, which means that the segregation rate becomes slower. Fig. 9 clearly illustrates this effect for the free-slip simulations: for all drag models the segregation becomes much slower with this correction (open symbols) than without it (closed symbols). In Fig. 7 it can be seen that this is also valid for systems with other boundary conditions.

From Fig. 9 we can observe that in the simulations without the correction factor the systems are almost completely segregated after one minute, whereas the segregation in the experiment is only about 64% after the same period of time. The degree of segregation in the simulation with the new drag

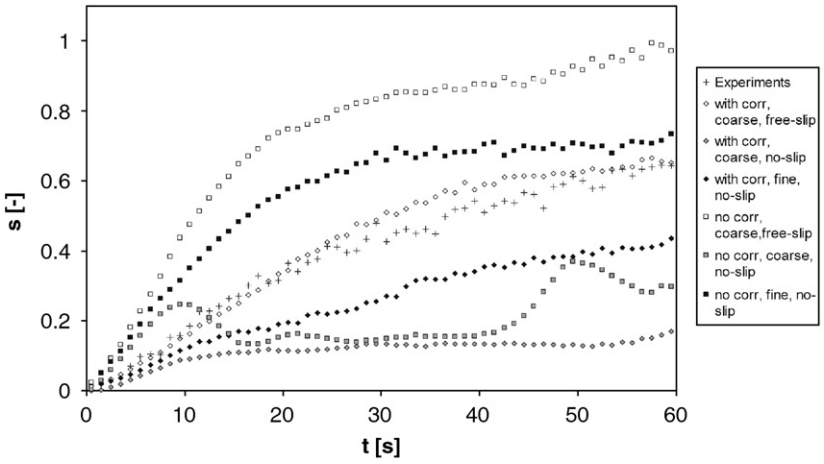

Fig. 7. Degree of segregation as a function of time in experiments and simulations with various boundary conditions. The drag force is calculated from the equation of Beetstra et al. (2006) in all simulations, the legend gives the other settings.

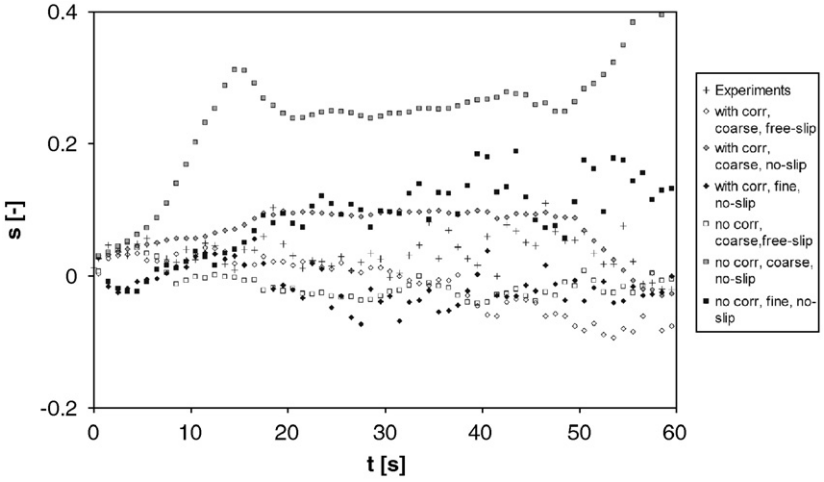

Fig. 8. Degree of segregation in the lateral direction as a function of time in experiments and simulations using various types of boundary conditions. The drag force is calculated from the equation of Beetstra et al. (2006) in all simulations, the legend gives the other settings.

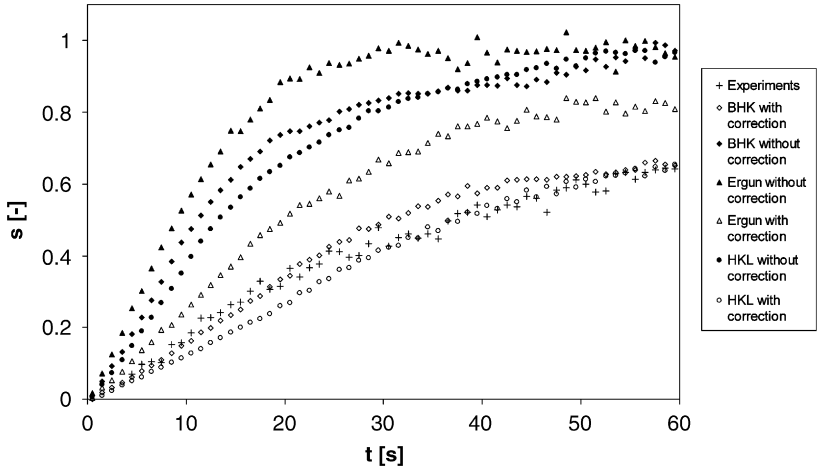

Fig. 9. Degree of segregation as a function of time in experiments and simulations with various drag models. All simulations were performed on a course grid with free-slip boundaries. The drag force is shown in the legend.

relation with polydispersity correction has a value of 65% after 1 min, and the rate at which the segregation occurs in the same simulation also compares very well with the trend observed in the experiment. The rate is better predicted with the new model than with the combination of Ergun and Wen and Yu equations with correction, while the performance of the model of Hill et al. (2001) is comparable to the new drag model obtained from this study.

5. Inversion

Layer inversion is a phenomenon that may occur in a fluidised bed that contains two (or more) particle species differing in both size and density, where the smaller particles have a larger density. At low liquid velocities gravity dominates the drag force, and the small but heavy particles will reside in the bottom section of the column. By raising the liquid velocity the drag force will increase, which results in a better mixing of the two phases. At the inversion velocity, the two phases are completely mixed. When the velocity is increased even further the drag forces dominate over gravity and the smaller particles will occupy the top section of the column, so that the order of the layers is inverted (see Fig. 10). The velocity at which the particles are mixed completely depends on the physical properties of both species and the composition of the mixture. Layer inversion occurs in mixtures containing three or more particle species as well, although in this case there is usually not a single inversion point (see e.g. Berres et al., 2005). The phenomenon has only been observed in liquid fluidisation, since this is usually more homogeneous than gas fluidisation. Although in theory inversion might occur in gas-fluidised beds, in practice the vigorous mixing due to bubbling action disturbs the segregation in layers, especially at high gas velocities.

The inversion phenomenon has been a topic of research interest for some years now. Moritomi et al. (1982, 1986) studied the inversion for a mixture of hollow char and glass particles as a function of mixture composition and diameter ratio. Their data have been used by other researchers to test the validity of

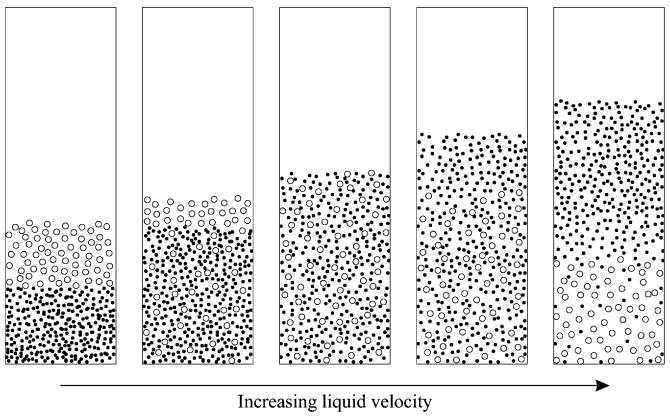

Fig. 10. Schematic representation of layer inversion in liquid fluidised beds, where the small particles have a higher density than the larger particles. The velocity is increased from left to right while the mixture composition is kept constant.

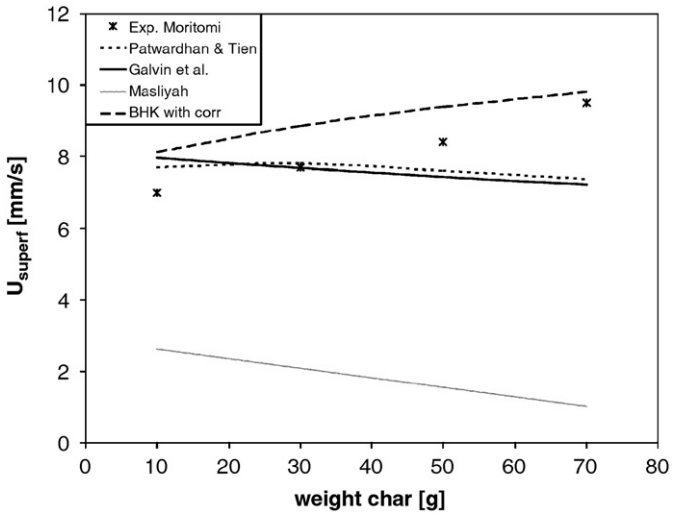

Fig. 11. Inversion velocity as a function of mixture composition calculated from various drag models, compared to the experiments of Moritomi et al. (1982).

their drag relations (see e.g. Patwardhan and Tien, 1985; Galvin et al., 1999; Biesheuvel, 2000). The systems that we use in our comparison are composed of glass particles with a diameter of $d_g = 0.163$ mm and char particles of $d_c = 0.775$ mm, with densities of 2450 and 1500 kg/m^3, respectively. The amount of glass particles in the column was fixed at 100 g, while the amount of coal was varied from 10 to 70 g in order to change the equilibrium composition of the mixture and thus its inversion velocity. The inversion point of a particle mixture is determined by calculating the porosity and liquid velocity at which an ideally mixed system of that composition is exactly in equilibrium, meaning that the forces originating from the fluid flow balance gravity for both particle species. Fig. 11 shows the inversion velocity of mixtures calculated from the drag model by Van der Hoef et al. (2005) for low Reynolds numbers, in combination with the correction for bidispersity, Eq. (8). The experimental results of Moritomi et al. (1986) are also shown, as well as the results from calculations using several literature models. It can be seen that the values calculated from the model of Masliyah (1979) are wide of the mark, where the other models, of Patwardhan and Tien (1985) and Galvin et al. (1999), predict more realistic values for the inversion velocity. However, they do not show the correct trend when the mixture composition is changed. The combination of the LBM derived drag relation and the polydispersity factor (Eq. (8)) shows the correct trend, although the inversion velocity in mixtures with a low amount of coal is overpredicted by about 16%.

6. Conclusions

In this work we have studied the effect of the gas–particle drag and the gas–wall boundary conditions in the numerical models of gas fluidisation in binary systems. The simulation results are compared with an experimental system of exactly the same size and with the same fluidisation conditions.

The general observation is that the boundary conditions for the side walls have a large effect on the segregation behaviour. The conclusion is that the no-slip boundary condition do not agree well with the realistic situation as observed in the experiments. It is probably best to model these system with free-slip conditions, since in that case the bed feels no influence from the walls and no unrealistic segregation patterns are formed. Note that since we are studying a quasi 2-D system (only one CFD grid cell in depth), we have not varied the boundary conditions for the front and the back wall, which are set to free-slip. For this reason, one could argue whether it is very useful to model the (much smaller) side walls as accurately as possible.

We have also investigated the effect of the gas–particle drag laws. We found that the correction factor for polydispersity, as derived from theory and LBM simulations, gives a significant improvement over drag models without this correction. The effect of the drag model itself is less pronounced, were the Ergun–Wen and Yu correlation gives the worst agreement with the experiments. It should be noted that the simulations with the correction for polydispersity show less lateral segregation compared to simulations without this correction, the reason of which is not completely evident. The change in the drag force may bring about subtle changes in the size and path of the bubbles, that are not large enough to observe in the snapshots. These changes could disturb the circulation patterns of the bed. A more thorough investigation into porosity and particle velocities in the bed is clearly required to confirm this.

Finally, we determined the inversion velocity of a liquid fluidised bed of binary particles, which differ both in size and density. We found that the drag force as derived from LBM simulations, including the correction for polydispersity, predicts the correct trend in the inversion velocity as a function of the mixture coefficient, although there is a systematic deviation of about 16%. In future work we intend to study such systems also by numerical simulation using the discrete particle model.

Acknowledgements

This work is part of the research programme of the ‘Stichting voor Fundamenteel Onderzoek der Materie (FOM)’, which is financially supported by the ‘Nederlandse Organisatie voor Wetenschappelijk Onderzoek (NWO)’. It was sponsored by the Stichting Nationale Computerfaciliteiten (National Computing Facilities Foundation, NCF) for the use of supercomputer facilities, with financial support from the Nederlandse Organisatie voor Wetenschappelijk Onderzoek (Netherlands Organization for Scientific Research, NWO).

References

Beetstra, R., van der Hoef, M.A., Kuipers, J.A.M., 2006. Drag force from lattice Boltzmann simulations of intermediate Reynolds number flow past mono- and bidisperse arrays of spheres. A.I.Ch.E. Journal, submitted for publication.

Berres, S., Bürger, R., Tory, E.M., 2005. On mathematical models and numerical simulation of the fluidization of polydisperse suspensions. Applied Mathematical Modelling 29, 159.

Biesheuvel, P.M., 2000. Comments on “A generalized empirical description for particle slip velocities in liquid fluidized beds” by K.P. Galvin, S. Pratten, G. Nguyen Tran Lam. Chemical Engineering Science 55, 1945.

Bokkers, G.A., van Sint Annaland, M., Kuipers, J.A.M., 2004. Mixing and segregation in a bidisperse gas–solid fluidised bed: a numerical and experimental study. Powder Technology 140, 176.

Enwald, H., Peirano, E., Almstedt, A.E., 1996. Eulerian two-phase flow theory applied to fluidization. International Journal of Multiphase Flow 22 (Suppl.), 21.

Ergun, S., 1952. Fluid flow through packed columns. Chemical Engineering Progress 48, 89.

Galvin, K.P., Pratten, S., Nguyen Tran Lam, G., 1999. A generalized empirical description for particle slip velocities in liquid fluidized beds. Chemical Engineering Science 54, 1045.

Goldschmidt, M.J.V., Link, J.M., Mellema, S., Kuipers, J.A.M., 2003. Digital image analysis measurements of bed expansion and segregation dynamics in dense gas-fluidised beds. Powder Technology 138, 135.

Hill, R.J., Koch, D.L., Ladd, J.C., 2001. Moderate-Reynolds-numbers flows in ordered and random arrays of spheres. Journal of Fluid Mechanics 448, 243.

Hoomans, B.P.B., 1999. Granular dynamics of gas–solid two-phase flows. Ph.D. Thesis, University of Twente, Enschede, The Netherlands.

Hoomans, B.P.B., Kuipers, J.A.M., Briels, W.J., van Swaaij, W.P.M., 1996. Discrete particle simulation of bubble and slug formation in a two-dimensional gas-fluidized bed: a hard sphere approach. Chemical Engineering Science 47, 99.

Masliyah, J.H., 1979. Hindered settling in a multi-species particle system. Chemical Engineering Science 34, 1166.

Moritomi, H., Iwase, T., Chiba, T., 1982. A comprehensive interpretation of solid layer inversion in liquid fluidised beds. Chemical Engineering Science 37, 1751.

Moritomi, H., Yamagishi, T., Chiba, T., 1986. Prediction of complete mixing of liquid-fluidized binary solid particles. Chemical Engineering Science 41, 297.

Patwardhan, V.S., Tien, C., 1985. Sedimentation and liquid fluidization of solid particles of different sizes and densities. Chemical Engineering Science 40, 1051.

Van der Hoef, M.A., Beetstra, R., Kuipers, J.A.M., 2005. Lattice Boltzmann simulations of low Reynolds number flow past mono- and bidisperse arrays of spheres: results for the permeability and drag force. Journal of Fluid Mechanics 528, 233.

Van der Hoef, M.A., Ye, M., van Sint Annaland, M., Kuipers, J.A.M., 2006. Multi-level modeling of gas-fluidized beds. Advances in Chemical Engineering 31, 65–149.

Wen, C.Y., Yu, Y.H., 1966. Mechanics of fluidization. Chemical Engineering Progress Symposium Series 62, 100.